HHS Public Access

Author manuscript

Neuroimage. Author manuscript; available in PMC 2021 November 15.

Published in final edited form as:

Neuroimage. 2021 November 15; 242: 118455. doi:10.1016/j.neuroimage.2021.118455.

Magnetization transfer weighted EPI facilitates cortical depth determination in native fMRI space

Yuhui Chai[a,*], **Linqing Li**[b], **Yicun Wang**[c], **Laurentius Huber**[d], **Benedikt A. Poser**[d], **Jeff Duyn**[c], **Peter A. Bandettini**[a,b]

[a] Section on Functional Imaging Methods, Laboratory of Brain and Cognition, NIMH, NIH, Bethesda 20892, MD, United States

[b] Functional MRI Core, NIMH, NIH, Bethesda, MD, United States

[c] Advanced MRI Section, Laboratory of Functional and Molecular Imaging, NINDS, NIH, Bethesda, MD, United States

[d] Maastricht Brain Imaging Center, Faculty of Psychology and Neuroscience, University of Maastricht, the Netherlands

Abstract

The increased availability of ultra-high field scanners provides an opportunity to perform fMRI at sub-millimeter spatial scales and enables *in vivo* probing of laminar function in the human brain. In most previous studies, the definition of cortical layers, or depths, is based on an anatomical reference image that is collected by a different acquisition sequence and exhibits different geometric distortion compared to the functional images. Here, we propose to generate the anatomical image with the fMRI acquisition technique by incorporating magnetization transfer (MT) weighted imaging. Small flip angle binomial pulse trains are used as MT preparation, with a flexible duration (several to tens of milliseconds), which can be applied before each EPI segment without constraining the acquisition length (segment or slice number). The method's feasibility was demonstrated at 7T for coverage of either a small slab or the near-whole brain at 0.8 mm isotropic resolution. Tissue contrast was found to be similar to that obtained with a state-of-art anatomical reference based on MP2RAGE. This MT-weighted EPI image allows an automatic reconstruction of the cortical surface to support laminar analysis in native fMRI space, obviating the need for distortion correction and registration.

Keywords

Cortical layer; Laminar; Layer; Depth; fMRI; Magnetization transfer

* Corresponding author. yuhui.chai@nih.gov (Y. Chai).

Declaration of Competing Interest

The authors declare no conflict of interest.

Supplementary materials

Supplementary material associated with this article can be found, in the online version, at doi:10.1016/j.neuroimage.2021.118455.

1. Introduction

With increased availability of ultra-high field (≥ 7T) human MRI scanners, functional magnetic resonance imaging (fMRI) spatial resolution has been pushed to the sub-millimeter domain, making it possible to resolve functional activity and connectivity across cortical layers. Despite the great potential of laminar fMRI research in humans, its widespread application is hampered by some technical constraints. One of the most important issues is how to determine cortical layers in native fMRI space, given the typically poor anatomical accuracy of fMRI scan techniques.

To assign cortical layers, one needs sufficient anatomical contrast to determine the gray matter (GM) boundaries with white matter (WM) and cerebrospinal fluid (CSF). Unfortunately, the typical gradient echo (GE) echo planar imaging (EPI) scan technique used for fMRI provides inadequate contrast between tissue types, and for this reason, boundaries are determined from separately acquired reference images. For this purpose, anatomical references based on T1-weighted Magnetization Prepared 2 Rapid Acquisition Gradient Echoes (MP2RAGE) are often acquired, which provide excellent GM-WM contrast, but different geometric distortions compared to the functional images. In this way, functional and anatomical information are generated in different image spaces, requiring co-registration between the two data sets and even distortion correction on the functional images. These post-processing steps not only induce spatial blurring of the functional data but also are in-adequately accurate at the cortical layer level. Therefore, it would be preferable to acquire both the anatomical reference and the fMRI data with the same scan technique.

A T1-weighted EPI image using inversion recovery (IR) preparation has been suggested for use as an anatomical reference in high-resolution fMRI, which has a matching distortion with the functional EPI data (Huber et al., 2017; Ikonomidou et al., 2005; Kashyap et al., 2018; Renvall et al., 2016). To ensure optimization of inversion time, this method has limited acquisition window and brain coverage when preceding a volume acquisition with a single inversion pulse. In high-resolution fMRI, the acquisition time for a single 3D volume image is relatively long. To improve the available sampling time, 3D-EPI volume acquisition can be split into multiple blocks and each of them is prepared with an IR module as in T1–2-3D-EPI (van der Zwaag et al., 2018), or 2D-EPI slices can be reordered differently after each IR as in multiple inversion-recovery time EPI (MI-EPI, 2D) (Renvall et al., 2016).

Here, we propose an alternative approach to generate the anatomical image by incorporating magnetization transfer (MT) weighted imaging with 3D-EPI. We apply the MT module before acquiring each k-space plane of 3D-EPI (a k_x -k_y plane of k-space acquired each time with a different k_z increment) without any in-plane segmentation, which works from a small slab (short acquisition length) to the near-whole brain coverage (long acquisition length). For functional imaging, we can turn off the MT preparation to collect blood-oxygen-level-dependent (BOLD) signal or add flow-sensitive gradients into the MT preparation to acquire a cerebral-blood-volume (CBV) and cerebral-blood-flow (CBF) weighted signal (details explained in Section 3.1.3 and Fig. S10), without changing the acquisition design. By doing so, the anatomical and functional images are naturally matched during acquisition.

This ensures the highest accuracy in defining cortical depth without the need for distortion correction and anatomical-functional co-registration.

2. Theory

2.1. Selective saturation of macromolecular hydrogen protons

In the human brain, a relatively large fraction of macromolecular ("macromolecules" is meant to include lipids) hydrogen protons (MP) (f ~0.2–0.3) is found in WM, primarily due to its high content of myelin, while this number is smaller in GM (f ~0.1) (van Gelderen et al., 2017). Through magnetization transfer with water hydrogen protons (WP), macromolecular protons can dramatically affect the MRI signal and thus different macromolecular-proton fractions will result in different MRI signal intensities. Binomial pulses have been used to selectively saturate macromolecular protons in MT studies for almost three decades (Hu et al., 1992; Yeung and Aisen, 1992) and used to be applied with a short length of large flip angle pulses (Stoeck et al., 2010; Wang et al., 2020). Here we modify it into a long stream of small flip angle (α, around 10°) binomial RF pulses (Fig. 1 A), to allow for a flexible combination with EPI acquisition of whole-brain images and meet the SAR limit at 7T scanner. For instance, we can apply as many as 247 pulse pairs with a total duration of 98.8 ms in every 1 s in the near-whole-brain imaging. While each pair of binomial pulses only slightly saturate the macromolecular protons, a cumulative saturation and transfer effect is achieved as the spin-lattice relaxation ($R_{1,WP}$ = 0.4 s^{-1}, $R_{1,MP}$ = 2 s^{-1}) and two-pools exchange rate (1.45 s^{-1}) (Wang et al., 2020) are much slower than the binomial pulse rate (larger than 1000 pulses/s in this study).

2.2. Sequence design

The sequence is implemented to acquire images alternately between MT-prepared and Control conditions (Fig. 1 C). In the MT-prepared condition, 3D-EPI segments (Poser et al., 2010) are interleaved with binomial pulse trains to image the signal of water protons affected by MT. Both the train length and pulse interval can be flexible, typically with 30–50 pulses and the interval of 0.2–1.1 ms. The corresponding saturtion frequency of binomial pulses (Fig. 1 B) needs to avoid the fat-water chemical shift, which can be achieved by constraining the pulse interval (τ) to be deviating from 1 / (2 × chemical shift). In control condition, the preparation module is switched off by setting α = 0°.

2.3. Generation of MT-weighted anatomical reference

The MT-weighted anatomical image is calculated as $\frac{S_{CTRL} - S_{MT}}{S_{MT}}$, where S_{CTRL} is the image signal in control condition, and S_{MT} is the image signal of MT-prepared condition (Fig. 2). This combination approach extracts the MT-saturated signal and removes the T_2^* contrast associated with the EPI acquisition.

3. Methods

3.1. MRI measurement

All participants gave their informed consent to participate in this study under the protocol 93-M-0170 (ClinicalTrials.gov identifier: NCT00001360) approved by the Institutional Review Board of the National Institute of Mental Health in Bethesda, MD. The experiments were performed on a MAGNETOM 7T scanner (Siemens Healthineers, Erlangen, Germany). A single-channel transmit/32-channel receive head coil (Nova Medical, Wilmington, MA, USA) was used for RF transmission and reception. A MT-3D-EPI sequence was implemented with acquisition parameters: excitation flip angle (FA) = 27° (constant across all segments), resolution around 0.8 mm isotropic, partial-Fourier of 7/8 (or 6/8 for the near-whole brain protocol) and GRAPPA 3. The 3D-EPI was segmented with the same number as the number of slices, acquiring a k_x - k_y plane of k-space after each shot with a different k_z increment. The terminology of "slice" was used here to indicate the 2D image plane of the read direction (x) by the 1st phase encoding direction (y). GRAPPA reconstruction was done on the FLASH autocalibration data (Talagala et al., 2016) and partial Fourier reconstruction was done with the projection onto convex sets (POCS) algorithm with 8 iterations (Haacke et al., 1991). Detailed parameters including those for MT preparation are listed in Table 1. Except for the purpose of RF power modulation, pulse duration in MT preparation was minimized to achieve the highest RF power allowed by the specific absorption rate (SAR) limit, in order to achieve an optimal tissue contrast (detailed reason in Fig. 3). To further maximize RF power of MT-preparation pulses under SAR limit, we didn't apply fat saturation or water-selective excitation. The fat signal was similar in CTRL and MT-prep images thus can be largely suppressed in computation of anatomical MT-weighted EPI images through $\frac{S_{CTRL} - S_{MT}}{S_{MT}}$.

3.1.1. Experiment 1: determining the contribution of MT effect to the WM-GM contrast—

To demonstrate that WM-GM contrast in MT-weighted EPI image is primarily determined by MT effect rather than the canonical T1 relaxation of a single exponential term, RF power of preparation pulses were modulated by varying pulse duration while keeping their FAs constant (Power = FA^2 / Pulse_duration). By doing so, the RF effect on the water protons stays the same while the macromolecular-proton pool is saturated at different levels. The WM-GM contrast was evaluated as $\frac{S_{WM} - S_{GM}}{(S_{WM} + S_{GM})/2}$, where S_{WM} and S_{GM} were the signals in WM and GM, respectively. This experiment of RF power modulation was conducted over three participants with partial brain coverage centering on the motor cortex. Detailed scan parameters are listed in Table 1.

Correspondingly, to theoretically evaluate how the MT effect modulates the WM-GM contrast across different RF powers compared to the canonical T1 relaxation, a single exponential T1 relaxation model and a two-pool model were adopted for Bloch simulations. In the canonical T1 relaxation model, both longitudinal and transverse relaxation are taken into account within each RF pulse duration in preparation, also between them and after them. In the two-pool model, water protons and macromolecular protons are considered as two separate magnetization groups. RF saturation of macromolecular protons is proportional

to the pulse power (Graham and Henkelman, 1997) and the two-pool cross-relaxation is characterized by the Bloch-McConnell equation (Henkelman et al., 1993; McConnell, 1958). The effect of excitation pulses in EPI acquisition on macromolecular protons is assumed to be negligible (Pike, 1996). The magnetization transfer between the two pools is considered throughout both the preparation and the acquisition time. Bloch equations of the two-pool model used in this study have been listed in Supplementary Materials.

3.1.2. Experiment 2: near-whole-brain MT-3D-EPI and its comparison with MP2RAGE—

To evaluate the MT-weighted EPI images in terms of WM-GM contrast, segmentation, and cortical depth properties, we scanned nine sessions over seven subjects (two of them being scanned twice) with the near-whole brain coverage (cerebellum not included). Detailed scan parameters are listed in Table 1 and the protocol is available at https://github.com/yuhuichai/MT3DEPI/blob/master/wholebrain_MT.pdf. As the T1-weighting approach has been used widely for anatomical imaging, we compared it with our MT-weighted EPI over those nine sessions in the perspective of tissue contrast. T1-weighted anatomical images were collected using a 3D Magnetization-Prepared 2 Rapid Acquisition Gradient Echo (MP2RAGE) sequence (Marques et al., 2010) with TI1/TI2/TR/TE = 800/2700/6000/3.02 ms, FA1/FA2 = 4°/5°, 224 sagittal slices, matrix size = 320 × 320, 0.7 mm isotropic resolution, scan time = 10 min 8 s. The MP2RAGE protocol is available at https://github.com/yuhuichai/MT3DEPI/blob/master/MP2RAGE.pdf. The raw data of near-whole-brain MT-3D-EPI and the skull-striped MP2RAGE images are available at https://osf.io/s4bqe/?view_only=dd8a1142ecd74d708526476b7776b717.

3.1.3. Experiment 3: laminar fMRI experiment in primary visual cortex—

As an example of using MT-weighted EPI for laminar fMRI analysis, we conducted an experiment to acquire both functional and anatomical data in primary visual cortex (V1) across three participants.

For functional measurements, we incorporated an integrated blood volume and perfusion (VAPER) contrast (Chai et al., 2020) by combining the blood-suppression module of DANTE (Delay Alternating with Nutation for Tailored Excitation) (Li et al., 2012) pulse trains with 3D-EPI. The sequence design is identical to MT-3D-EPI except for adding a gradient in each pulse interval of MT preparation (Fig. S10). In VAPER-3D-EPI, a corresponding control measurement was collected every other volume TR as in the MT-3D-EPI sequence scheme, whose signal can be considered as a conventional gradient echo BOLD. All acquisition parameters of VAPER-3D-EPI are identical with MT-3D-EPI as listed in Table 1, except for volume TR = 3150 ms and scan time = 31 min 30 s (protocol available at https://github.com/yuhuichai/MT3DEPI/blob/master/VAPER_V1.pdf). Volume TR of VAPER-3D-EPI is longer than that of MT-3D-EPI as the inserted gradient pulses increase the preparation time. For the task, a 30-min checkerboard flickering (contrast reversing rate, 10 Hz) was presented in a block-designed manner (30-s stimulation / 30-s rest).

3.2. Data analysis

3.2.1. Preprocessing—1) Motion correction was applied to the images of control and MT-prepared volumes in MT-3D-EPI imaging, together with the images of control and DANTE-prepared volumes in VAPER-3D-EPI imaging when functional measurements were conducted in the same session in Experiment 3. This strategy of applying motion correction to all runs acquired by different sequences works only when an identical EPI acquisition is applied. We used SPM12 (Wellcome Trust Center for Neuroimaging, London, UK) for this motion estimation and correction, and the script is available at https://github.com/yuhuichai/MT3DEPI/blob/master/mc_run.m. **2) Time points were censored** from further analysis (e.g., generating anatomical MT-weighted EPI images, or functional regression analysis) whenever the Euclidean norm of the motion derivatives exceeded 0.4 mm (based on the motion parameters estimated by SPM12) or when at least 10% of image voxels were seen as outliers from the trend. The script for this step is available at https://github.com/yuhuichai/MT3DEPI/blob/master/motion_censor.sh. **3)** The **time series of MT-weighted anatomical images** were generated via subtraction of the paired control and MT-prepared time points and further division by the MT-prepared images. **VAPER time series** were generated via subtraction of the paired control and DANTE-prepared time points and further division of the control. The mean MT-weighted anatomical images were further denoised using ANTs program *DenoiseImage* and then used for histogram analysis and cortical surface/depth reconstruction. The script of this step is available at https://github.com/yuhuichai/MT3DEPI/blob/master/vaper.sh

3.2.2. SNR analysis of MT-weighted EPI image—The signal-to-noise ratio (SNR) was evaluated by averaging separately the even and odd numbered MT-weighted anatomical images in the time series ($S_{anat} = \frac{S_{CTRL} - S_{MT}}{S_{MT}}$, where S_{CTRL} is the image signal in control condition, and S_{MT} is the image signal of MT-prepared condition), and adding and subtracting these two average images to obtain sum and difference images. The SNR was calculated as the ratio of the mean value from a region-of-interest (ROI) in the sum image and the standard deviation in the same ROI in the difference image. This method has been used to calculate SNR for fMRI images (Glover and Lai, 1998; Kruger et al., 2001). The script used for SNR computation is available at https://github.com/yuhuichai/MT3DEPI/blob/master/snr.sh.

3.2.3. Background noise removal—In generation of anatomical MT-weighted EPI images through $\frac{S_{CTRL} - S_{MT}}{S_{MT}}$, the noise signal can be amplified when the denominator tends towards zero. This is known as *salt-and-pepper* noise (O'Brien et al., 2014), and it is most common in background non-brain region. When the noise voxels are next to the cortical surface or the brain tissue, the brain segmentation algorithm often mistakenly includes these non-cortex noise voxels as part of the brain and significantly affects the accuracy of cortical surface reconstruction. To solve this issue, we combined two following steps.

First, we used the mean image of CTRL from MT-3D-EPI measurement to determine the mask of the brain region. Images of CTRL-3D-EPI are basically $T2^*$-weighted BOLD images, in which the signal intensities in background non-brain region are much smaller (darker in image) compared to that in brain region. Thus, the mask based on CTRL volumes can help remove most of the noise outside the brain.

Second, we added a constant number β to the equation of generating anatomical MT-weighted image:

$$S_{ANAT} = \frac{S_{CTRL} - S_{MT}}{S_{MT} + \beta}$$

where S_{CTRL} is the signal in control volume, and S_{MT} is the signal of MT-prepared volume. When the S_{MT} is very low as in noise region, the constant β will dominate the ratio calculation and suppress the output value in S_{ANAT}. When S_{MT} is large as in brain region, β should have minimal impact on the ratio calculation. The choice of β depends on the mean signal intensity in brain and background noise regions. We have evaluated different β levels as in Fig. 5. This idea of background noise suppression here was inspired by that in MP2RAGE (O'Brien et al., 2014).

3.2.4. Brain segmentation and cortical surface/depth reconstruction—For the near-whole-brain MT-weighted EPI images, WM/GM segments and cortical surface were generated using the FreeSurfer program *recon-all*. As the cerebellum was not included in our near-whole-brain EPI coverage and it is needed for a proper atlas alignment with *reconall*, we added this missing part from the registered MP2RAGE image to the MT-weighted EPI image. The cerebellum was not included in the resulted cortical surface and thus all cortical surface/depth related analysis in EPI space was solely based on EPI data. The processing script for this step is available at https://github.com/yuhuichai/MT3DEPI/blob/master/reconall_mtepi.sh. In the absence of a whole-brain MP2RAGE, we would have to increase the coverage of MT-3D-EPI to include cerebellum which would extend the acquisition time of the MT-3D-EPI.

With the cortical surface automatically generated by FreeSurfer, we calculated cortical depths based on the equi-volume approach (Waehnert et al., 2014) using the LAYNII software suite (Huber et al., 2021) and divided the cortex into 20 equi-volume layers. Since at the acquired spatial resolution (0.8 mm) a voxel can lie across several cortical depths, MT-weighted anatomical images were upsampled by a factor of 4 for the cortical layer reconstruction. The number of 20 layers was chosen in order to improve layer profile visualization and to minimize partial voluming between neighboring voxels (Huber et al., 2018). For a lower number of layers, multiple voxels with centroids across a wider range of cortical depths would have been binned into the same layer, which would have resulted in loss of resolution. This layer computation was conducted in EPI volume space (not surface) and the processing script is available at https://github.com/yuhuichai/MT3DEPI/blob/master/layer_seg_MT3DEPI.sh. In the whole context of this study, we used the term 'laminar' or 'layer' to indicate a measurement taken along the cortical depth, as opposed to the cytoarchitectonically defined cortical layers.

The brain segmentation and cortical surface/depths reconstruction for MP2RAGE images were computed in the same manner in its own image space, without the need of adding cerebellum.

3.2.5. Comparison of tissue contrasts and image intensities across cortical depths in MT-3D-EPI vs. MP2RAGE—

1) Intensity normalization: As the image intensity values in the respective anatomical data are in very different ranges across MT-3D-EPI and MP2RAGE, we applied the AFNI (Cox, 1996) program *3dUnifize* (being modified to allow the intensity normalization in negative voxels, script available at https://github.com/yuhuichai/MT3DEPI/blob/master/3dUnifize_nomask.c) to normalize image intensity. The resulting anatomical images have WM intensity approximately uniformized across space and scaled to peak at about 1000. **2) Matching brain mask across different image space:** To compare the image properties between MT-3D-EPI and MP2RAGE in same brain regions, we computed the co-registration matrix between MP2RAGE and MT-weighted EPI images using ANTs program *antsRegistration* (processing script available at https://github.com/yuhuichai/MT3DEPI/blob/master/align_mp2rage2epi.sh), and then apply this transform to ensure same masking of the brain region. Inside the same brain mask, all ROIs including WM, GM, Broadman areas and visual areas, were defined in their own data of either EPI or MP2RAGE. **3) Histogram analysis:** We computed one-dimensional (1D) histograms for GM, WM, CSF and whole brain regions to show the number of voxels at different normalized signal intensities. **4) Image intensities across cortical depths:** In each ROI (BA2/3/4/6, V1/2, whole brain GM), the mean signal intensity of all voxels in each layer was extracted and plotted across different layers. All ROIs were created by default when FreeSurfer program *recon-all* was run.

3.2.6. Analysis of layer-fMRI response in V1 for Experiment 3—

Statistical analysis was performed separately for BOLD and VAPER data which were concurrently acquired by VAPER-3D-EPI sequence, using AFNI program (Cox, 1996) *3dDeconvolve*. In order to use beta weights associated with each covariate as percent signal changes, all voxel-wise time series of each contrast were normalized by each voxel's mean signal across time before feeding to the regression model. In addition, to avoid the weighting of the baseline signal intensities on the resulted depth-dependent response profile, we also computed the absolute signal changes of arbitrary unit (a.u.) as the regression coefficient without the normalization by mean.

As the automatic surface reconstruction using FreeSurfer doesn't work with a small brain coverage, CSF/GM borders and GM/WM borders in the calcarine sulcus were manually drawn on the MT-weighted EPI image. Cortical layers were computed in the same way as in the near-whole-brain EPI images based on the manually-draw cortical borders. To calculate signal changes across layers, all voxels were included in each layer ROI without any thresholding.

4. Results

Fig. 3 shows the WM-GM contrast under different RF powers of MT preparation. The measured WM-GM contrast (green circle in Fig. 3 B) can be predicted well by the

two-pool model of MT effect (red curve in Fig. 3 B). Higher RF power results in more macromolecular-proton saturation which transfers to water protons, and eventually leads to a larger WM-GM contrast due to their difference in macromolecular-protons fraction. On the contrary, when only considering the single exponential T1 relaxation of GM and WM, there is negligible variation of WM-GM contrast (blue curve in Fig. 3 B) as FA is constant, which does not match the experimental observation.

Fig. 4 shows the original near-whole-brain MT-weighted EPI images (without masking and denoising) and their SNRs after averaging different volume numbers. By averaging more measurements, SNRs in GM and WM increase, which is the same for the SNR difference between GM and WM (Fig. 4 B, top). Please note the SNR here refers to the signal of $S_{anat} = \frac{S_{CTRL} - S_{MT}}{S_{MT}}$ and the noise has been amplified compared to the original EPI image signal, mainly because of the ratio computation. The SNRs of the original control and MT-prepared EPI images are much higher (SNR in GM / WM = 87 ± 9 / 106 ± 10 for control EPI, 76 ± 5 / 82 ± 7 for MT-prepared EPI, when averaging over 50 measurements). In addition, the SNR in GM or WM was the average value of SNRs in all GM or WM voxels. From top to bottom slices, the SNR dramatically decreases due to the weak coil sensitivity and B1 transmission efficiency in bottom regions of the head (Fig. 4 B, bottom). To ensure a sufficient SNR, the MT-weighted EPI images used for a further cortical surface/depth reconstruction were averaged over 50 measurements in following results. Although this is even more time-consuming than the typical MP2RAGE acquisition (10 min 8 s), it is worth noting that the main motivation for an anatomical reference in native fMRI space is because of the matching image space (distortions) to the functional EPI data. Considering both time efficiency and SNR, we recommend averaging 40–50 measurements in future layer fMRI studies using this method.

In Fig. 5, we applied the background noise suppression to anatomical MT-weighted images with different β levels, through the equation of $S_{ANAT} = \frac{S_{CTRL} - S_{MT}}{S_{MT} + \beta}$. In original anatomical MT-weighted EPI images ($\beta = 0$), noise signal can be amplified when the denominator (S_{MT}) tends towards zero. This noise has a “salt-and-pepper” characteristic, distributed throughout the background non-brain region, in areas non-cortical but touching cortical surface and in some low-SNR brain voxels (a few examples marked by yellow arrows in upper left of Fig. 5 A). By simply adding a constant β to the denominator of the ratio computation, this noise could be largely suppressed (Fig. 5 A). Larger β led to better noise suppression, but slightly worse GM/WM contrast (Fig. 5 B). In this study, the mean S_{MT} in areas of background non-brain, GM and WM were 68 ± 22 (mean ± SD across 9 sessions), 299 ± 17 and 420 ± 28, respectively. We recommend a use of $\beta = 100$ here, as this value is (1) larger than the background signal intensity thus being able to suppress background noise, (2) much smaller than the mean intensity in brain tissue thus to minimize the impact on the computation in tissue voxels. The impact of background noise suppression on the accuracy of cortical surface reconstruction can be found in Fig. S8.

Fig. 6 show the results of comparing MT-weighted EPI and MP2RAGE images. The tissue contrast looks very similar in the images of these two techniques. Accordingly, the image

intensity histograms of the GM and WM voxels are similarly well separated, as shown in Fig. 6 C. The histograms counted voxels in the GM/WM (Fig. 6 C, top) and the whole brain (Fig. 6 C, bottom) regions over 9 sessions from 7 subjects. The ROIs of GM and WM were determined automatically based on the brain segmentation results (method detail in Section 3.2.4) for either MP2RAGE or MT-weighted EPI images. Fig. 6 B shows an example of the GM/WM segmentation from the MT-weighted EPI image in one representative subject. Besides the similar tissue contrast, the signals in arteries and CSF are better suppressed in MT-weighted EPI than MP2RAGE. For example, the signals of arteries voxels in insula areas marked by cyan arrows appear bright in MP2RAGE while suppressed in MT-weighted EPI images (Fig. 6 A). Furthermore, the intensity histograms of GM and CSF voxels are better separated in MT-weighted EPI images, suggesting a better contrast between CSF and GM compared to MP2RAGE, as shown in Fig. S1.

In addition, one key distinction was observed in subcortical structures (Fig. S5). Areas of pallidum, putamen and thalamus are better distinguishable from the surrounding WM in MT-weighted EPI images compared to MP2RAGE images. This is due to a rich iron density in those subcortical structures which shortens the GM T1 and thus reduces the T1 difference between GM and WM, while MT contrast is typically less sensitive to iron. This finding is in agreement with previous research of MT contrast (Helms et al., 2009; Yarnykh, 2016).

With the near-whole-brain MT-weighted EPI images, we are able to run a cortical surface reconstruction using FreeSurfer (Fischl, 2012) and then a cortical layer computation using LAYNII (Huber et al., 2021) automatically. Fig. 7 A and 7 B show the generated pial/WM surfaces and cortical depths, respectively, in three representative slices from superior (slice 1) to inferior of the brain (slice 3). At each cortical depth, we extracted the mean image intensity and its difference with adjacent depths across different ROIs, including BA2/3/4/6, V1/2, and the whole cerebral cortex, as shown in Fig. S6. Generally, the laminar profiles of the signal intensity appear similar in MT-weighed EPI and MP2RAGE images. In areas whose cortical surfaces are surrounded by more CSF, such as BA2/3/4, the image intensity transition across GM/CSF border is sharper in MT-weighed EPI images than MP2RAGE, which is also shown as a stronger spike in the profile of the intensity difference with adjacent layers for MT-weighted EPI. This is likely due to a stronger contrast between CSF and GM in MT-weighted EPI images as shown in Fig. S1.

Fig. 8 shows an example of extracting laminar activity in native fMRI space when functional BOLD/VAPER and anatomical MT-weighted images were acquired using an identical EPI acquisition (sequence diagrams for each contrast and their representative images shown in Fig. S10). In each participant, cortical depths in calcarine sulcus were determined based on the underlay MT-weighted EPI images. Their right shows the corresponding laminar profiles of BOLD and VAPER activity during visual checkerboard stimulation. Because normalization with different baseline signals can introduce different weighting of inverse baseline signal intensity into the laminar profile, here we show results of both the percent signal changes (voxel-wise time series normalized by its mean) and the absolute signal changes (without signal normalization). The findings are consistent across participants regardless of the signal normalization: while BOLD response is weighted toward cortical surface as expected by the draining vein effect (signal change decreases from the cortical

surface near CSF to the deep cortical depth near WM as shown in red curves), VAPER signal changes peak around the middle cortical depths (signal changes shown by blue curves appear highest at the middle depths of gray matter (mid-GM)). This peak response in the middle layers of V1 during visual stimulation has also been seen in animal layer fMRI research using cerebral blood volume/flow measurement (Jin and Kim, 2008), which reflects the feedforward input from the LGN.

5. Discussion

5.1. Prospects and challenges of MT-weighted EPI compared to T1-weighted EPI

The concept of anatomical reference in native fMRI space has been proposed before and studied mostly in T1-weighted EPI (Renvall et al., 2016; van der Zwaag et al., 2018). In this study we suggested an alternative approach, termed MT-weighted EPI, which has both benefits and challenges compared to previous T1-weighted EPI approach.

Our MT-3D-EPI approach can have two main advantages over the IR-prepared T1-weighted 3D-EPI (T1–3D-EPI): (1) The prepared magnetization at the beginning of each EPI segment in the MT-3D-EPI sequence is closer to the steady-state than that in the T1–3D-EPI, leading to a smaller blurring kernel being applied along the 2nd phase encoding direction (Fig. S3). In T1–3D-EPI, each IR is followed by a series of EPI segments, and the signals at different segments vary according to the different delay time between the IR pulse and the acquisition of each segment. In contrast, in MT-3D-EPI, the binomial pulse train can be evenly distributed before each segment of 3D-EPI, thus the measured signal can reach a steady state and vary less across segments. (2) There is a more flexible trade-off between the acquisition length and the EPI-segmentation strategy in MT-3D-EPI than T1–3D-EPI. In T1-weighted EPI using IR, optimal contrast is obtained at a limited range of inversion recovery times, which limits the EPI acquisition length after each IR. On the other hand, it is time and SAR inefficient to apply an inversion pulse before each EPI segment. This leads to the need of different segmentations of T1–3D-EPI for images with different matrix sizes (e.g., one inversion pulse followed by the acquisition of a whole volume for a small coverage, or splitting k-space of each volume across multiple IR-blocks), which depends on the chosen imaging coverages or spatial resolutions. In MT-3D-EPI, because of the flexibility in the MT module duration (several to tens of milliseconds) and the small flip angle design in our study, the MT preparation can be applied before each excitation shot regardless of various EPI segmentation schemes and the acquisition length. Extending from a few slices toward a whole brain coverage, the EPI design does not need to change. Although the flexible segmentation of 3D-EPI is not a limiting factor with techniques like Skipped-CAIPI (Stirnberg and Stocker, 2021), it is still an advantage to be less restricted on the acquisition design with MT-3D-EPI.

Along with these benefits, our MT weighting approach suffers from the susceptibility to the transmit RF field inhomogeneities. In ultrahigh field, the transmitted RF magnetic field can be quite inhomogeneous over the brain. In our MT-weighted EPI image, the WM-GM contrast is dependent on the RF power and thus it varies with different RF inhomogeneities. This is less an issue for the IR-prepared T1-weighted approach when an adiabatic inversion pulse is used. We would like to point out, however, that the increased WM-GM contrast

with an increasing RF power of MT preparation looks like a sigmoid curve as shown in Fig. 3 B. As long as the RF power of MT preparation is sufficient enough, the WM-GM contrast approaches a plateau and the RF inhomogeneity induced contrast variation goes down. Therefore, in current study, we strove to use the largest RF power for MT preparation allowed by the SAR limit. In future work, we will optimize it further by B1 shimming using parallel transmission or using dielectric pad (Teeuwisse et al., 2012; Vu et al., 2015) to enhance B1 transmission efficiency for brain regions like temporal lobe and visual cortex.

5.2. Contrast of T1 vs. MT

In many studies (Gochberg et al., 1997; Prantner et al., 2008; van Gelderen et al., 2016; Wang et al., 2020), it has been shown that the tissue longitudinal relaxation is largely a manifest of MT effect. Both T1 and MT contrasts are thought to be proxies of myelin content and the myelin concentration difference in WM and GM is the principal source of the tissue contrast in either T1 or MT weighted images. Exceptions are, mostly, paramagnetic relaxation effects associated with iron (Wang et al., 2020). This may affect T1 contrast more than MT contrast. For this reason, midbrain iron containing regions look different in these two contrasts, which is also shown in our study (Fig. S5). To some extent, this can also be seen in motor cortex and visual cortex, of which deeper layers have higher iron (Duyn et al., 2007; Fukunaga et al., 2010). The latter reduces the contrast at the GM-WM boundary in T1-weighted images. This can be a potential advantage of MT-based contrast used for laminar reference imaging although we didn't observe it in current study.

In terms of mechanism modeling, T1 relaxation is usually assumed to be a single exponential term and not affected by RF power, whereas the two-pool MT model separates RF effects on water protons and macromolecular protons, having the advantage of concerning RF power. In cases of variable powers across measurements, the discrepancy in image contrast is much better characterized by the MT mechanism. In our MT-weighted EPI imaging, the key parameter to optimize anatomical contrast is the RF power in the preparation, such that a higher power leads to a larger WM-GM contrast. This phenomenon further supports us to attribute the anatomical images in our study to be MT weighting.

6. Conclusion

In this study, we incorporated MT weighting into a 3D-EPI sequence to acquire an anatomical reference in the same space as the fMRI data. The method's feasibility was demonstrated at 7T for coverage of either a small slab or the near-whole brain at 0.8 mm isotropic resolution. Similar tissue contrast was obtained compared to MP2RAGE, as evidenced by the separation of GM and WM peaks in the image intensity histograms. This allows us to reconstruct cortical surface and compute cortical depth using well established programs (i.e., FreeSurfer, LAYNII) in native EPI space. By using an identical EPI acquisition for both functional and anatomical imaging, all fMRI analysis including the laminar part can be performed in native fMRI space, without the need for distortion correction and registration, thus preserving the high spatial resolution in the original data.

Supplementary Material

Refer to Web version on PubMed Central for supplementary material.

Acknowledgements

This work is supported by the Intramural Research Program of the National Institute of Mental Health (annual report ZIAMH002783). Yicun Wang and Jeff Duyn are supported by the Intramural Research Program of the National Institute of Neurological Disorders and Stroke. Laurentius Huber is funded by the NWO VENI project 016.Veni.198.032. Benedikt Poser is partially funded by the NWO VIDI grant 16.Vidi.178.052 and by the National Institute for Health grant (R01MH/111444). We acknowledge NIH Fellows Editorial Board for the editorial assistance.

References

Chai Y, Li L, Huber L, Poser BA, Bandettini PA, 2020. Integrated VASO and perfusion contrast: a new tool for laminar functional MRI. Neuroimage 207, 116358. [PubMed: 31740341]

Cox RW, 1996. AFNI: software for analysis and visualization of functional magnetic resonance neuroimages. Comput. Biomed. Res. 29, 162–173. [PubMed: 8812068]

Duyn JH, van Gelderen P, Li TQ, de Zwart JA, Koretsky AP, Fukunaga M, 2007. High-field MRI of brain cortical substructure based on signal phase. Proc. Natl. Acad. Sci. USA 104, 11796–11801. [PubMed: 17586684]

Fischl B, 2012. FreeSurfer. Neuroimage 62, 774–781. [PubMed: 22248573]

Fukunaga M, Li TQ, van Gelderen P, de Zwart JA, Shmueli K, Yao B, Lee J, Maric D, Aronova MA, Zhang G, Leapman RD, Schenck JF, Merkle H, Duyn JH, 2010. Layer-specific variation of iron content in cerebral cortex as a source of MRI contrast. Proc. Natl. Acad. Sci. USA 107, 3834–3839. [PubMed: 20133720]

Glover GH, Lai S, 1998. Self-navigated spiral fMRI: interleaved versus single-shot. Magn. Reson. Med. 39, 361–368. [PubMed: 9498591]

Gochberg DF, Kennan RP, Gore JC, 1997. Quantitative studies of magnetization transfer by selective excitation and T1 recovery. Magn. Reson. Med. 38, 224–231. [PubMed: 9256101]

Graham SJ, Henkelman RM, 1997. Understanding pulsed magnetization transfer. J. Magn. Reson. Imaging 7, 903–912. [PubMed: 9307918]

Haacke EM, Lindskog ED, Lin W, 1991. A fast, iterative, partial-Fourier technique capable of local phase recovery. J. Magn. Reson. 92, 126–145.

Helms G, Draganski B, Frackowiak R, Ashburner J, Weiskopf N, 2009. Improved segmentation of deep brain grey matter structures using magnetization transfer (MT) parameter maps. Neuroimage 47, 194–198. [PubMed: 19344771]

Henkelman RM, Huang X, Xiang QS, Stanisz GJ, Swanson SD, Bronskill MJ, 1993. Quantitative interpretation of magnetization transfer. Magn. Reson. Med. 29, 759–766. [PubMed: 8350718]

Hu BS, Conolly SM, Wright GA, Nishimura DG, Macovski A, 1992. Pulsed saturation transfer contrast. Magn. Reson. Med. 26, 231–240. [PubMed: 1325023]

Huber L, Handwerker DA, Jangraw DC, Chen G, Hall A, Stuber C, Gonzalez–Castillo J, Ivanov D, Marrett S, Guidi M, Goense J, Poser BA, Bandettini PA, 2017. High-resolution CBV-fMRI allows mapping of laminar activity and connectivity of cortical input and output in human M1. Neuron 96, 1253–1263 e1257. [PubMed: 29224727]

Huber L, Tse DHY, Wiggins CJ, Uludag K, Kashyap S, Jangraw DC, Bandettini PA, Poser BA, Ivanov D, 2018. Ultra-high resolution blood volume fMRI and BOLD fMRI in humans at 9.4 T: capabilities and challenges. Neuroimage 178, 769–779. [PubMed: 29890330]

Huber LR, Poser BA, Bandettini PA, Arora K, Wagstyl K, Cho S, Goense J, Nothnagel N, Morgan AT, van den Hurk J, Muller AK, Reynolds RC, Glen DR, Goebel R, Gulban OF, 2021. LayNii: a software suite for layer-fMRI. Neuroimage 237, 118091. [PubMed: 33991698]

Ikonomidou VN, van Gelderen P, de Zwart JA, Fukunaga M, Duyn JH, 2005. Optimizing brain tissue contrast with EPI: a simulated annealing approach. Magn. Reson. Med. 54, 373–385. [PubMed: 16032676]

Jin T, Kim SG, 2008. Cortical layer-dependent dynamic blood oxygenation, cerebral blood flow and cerebral blood volume responses during visual stimulation. Neuroimage 43, 1–9. [PubMed: 18655837]

Kashyap S, Ivanov D, Havlicek M, Poser BA, Uludag K, 2018. Impact of acquisition and analysis strategies on cortical depth-dependent fMRI. Neuroimage 168, 332–344. [PubMed: 28506874]

Kruger G, Kastrup A, Glover GH, 2001. Neuroimaging at 1.5 T and 3.0 T: comparison of oxygenation-sensitive magnetic resonance imaging. Magn. Reson. Med. 45, 595–604. [PubMed: 11283987]

Li LQ, Miller KL, Jezzard P, 2012. DANTE-prepared pulse trains: a novel approach to motion-sensitized and motion-suppressed quantitative magnetic resonance imaging. Magn. Reson. Med. 68, 1423–1438. [PubMed: 22246917]

Marques JP, Kober T, Krueger G, van der Zwaag W, Van de Moortele PF, Gruetter R, 2010. MP2RAGE, a self bias-field corrected sequence for improved segmentation and T1-mapping at high field. Neuroimage 49, 1271–1281. [PubMed: 19819338]

McConnell HM, 1958. Reaction rates by nuclear magnetic resonance. J. Chem. Phys. 28, 430–431.

O'Brien KR, Kober T, Hagmann P, Maeder P, Marques J, Lazeyras F, Krueger G, Roche A, 2014. Robust T1-weighted structural brain imaging and morphometry at 7T using MP2RAGE. PLoS One 9, e99676. [PubMed: 24932514]

Pike GB, 1996. Pulsed magnetization transfer contrast in gradient echo imaging: a two-pool analytic description of signal response. Magn. Reson. Med. 36, 95–103. [PubMed: 8795027]

Poser BA, Koopmans PJ, Witzel T, Wald LL, Barth M, 2010. Three dimensional echo-planar imaging at 7 Tesla. Neuroimage 51, 261–266. [PubMed: 20139009]

Prantner AM, Bretthorst GL, Neil JJ, Garbow JR, Ackerman JJ, 2008. Magnetization transfer induced biexponential longitudinal relaxation. Magn. Reson. Med. 60, 555–563. [PubMed: 18759367]

Renvall V, Witzel T, Wald LL, Polimeni JR, 2016. Automatic cortical surface reconstruction of high-resolution T1 echo planar imaging data. Neuroimage 134, 338–354. [PubMed: 27079529]

Stirnberg R, Stocker T, 2021. Segmented K-space blipped-controlled aliasing in parallel imaging for high spatiotemporal resolution EPI. Magn. Reson. Med. 85, 1540–1551. [PubMed: 32936488]

Stoeck CT, Hu P, Peters DC, Kissinger KV, Goddu B, Goepfert L, Ngo L, Manning WJ, Kozerke S, Nezafat R, 2010. Optimization of on-resonant magnetization transfer contrast in coronary vein MRI. Magn. Reson. Med. 64, 1849–1854. [PubMed: 20938974]

Talagala SL, Sarlls JE, Liu SY, Inati SJ, 2016. Improvement of temporal signal–to-noise ratio of GRAPPA accelerated echo planar imaging using a FLASH based calibration scan. Magn. Reson. Med. 75, 2362–2371. [PubMed: 26192822]

Teeuwisse WM, Brink WM, Webb AG, 2012. Quantitative assessment of the effects of high-permittivity pads in 7 Tesla MRI of the brain. Magn. Reson. Med. 67, 1285–1293. [PubMed: 21826732]

van der Zwaag W, Buur PF, Fracasso A, van Doesum T, Uludag K, Versluis MJ, Marques JP, 2018. Distortion-matched T1 maps and unbiased T1-weighted images as anatomical reference for high-resolution fMRI. Neuroimage 176, 41–55. [PubMed: 29665420]

van Gelderen P, Jiang X, Duyn JH, 2016. Effects of magnetization transfer on T1 contrast in human brain white matter. Neuroimage 128, 85–95. [PubMed: 26724780]

van Gelderen P, Jiang X, Duyn JH, 2017. Rapid measurement of brain macromolecular proton fraction with transient saturation transfer MRI. Magn. Reson. Med. 77, 2174–2185. [PubMed: 27342121]

Vu AT, Auerbach E, Lenglet C, Moeller S, Sotiropoulos SN, Jbabdi S, Andersson J, Yacoub E, Ugurbil K, 2015. High resolution whole brain diffusion imaging at 7T for the Human Connectome Project. Neuroimage 122, 318–331. [PubMed: 26260428]

Waehnert MD, Dinse J, Weiss M, Streicher MN, Waehnert P, Geyer S, Turner R, Bazin PL, 2014. Anatomically motivated modeling of cortical laminae. Neuroimage 93 (Pt 2), 210–220. [PubMed: 23603284]

Wang Y, van Gelderen P, de Zwart JA, Duyn JH, 2020. B0-field dependence of MRI T1 relaxation in human brain. Neuroimage 213, 116700. [PubMed: 32145438]

Yarnykh VL, 2016. Time-efficient, high-resolution, whole brain three-dimensional macromolecular proton fraction mapping. Magn. Reson. Med. 75, 2100–2106. [PubMed: 26102097]

Yeung HN, Aisen AM, 1992. Magnetization transfer contrast with periodic pulsed saturation. Radiology 183, 209–214. [PubMed: 1549673]

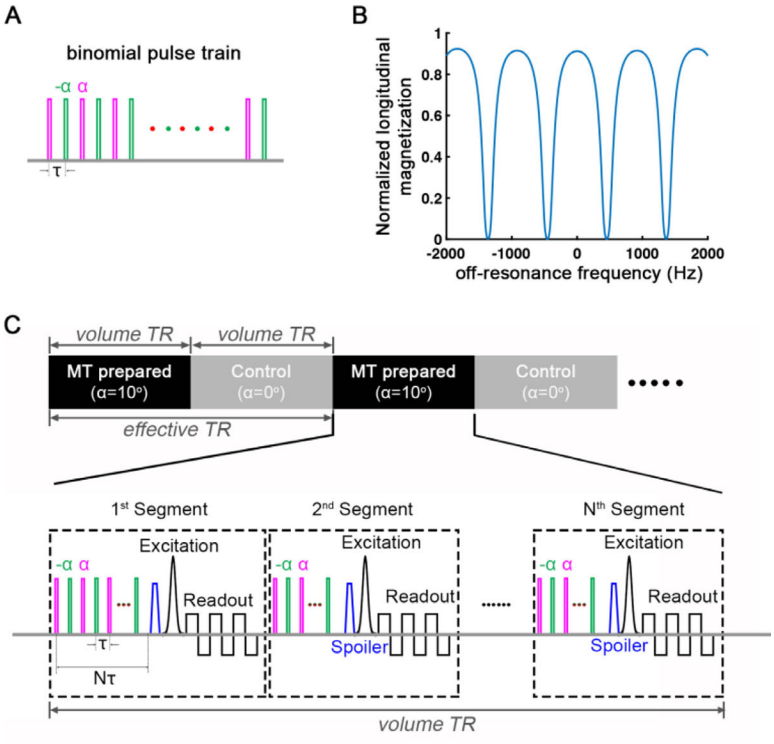

Fig. 1.

Binomial pulse train and its combination with 3D-EPI acquisition. (A) Binomial pulse train consists of a series of low flip-angle (a, around 10°) pulses with alternating polarity (magenta rectangle pulse for a, green rectangle pulse for - a). (B) The spectrum for a binomial RF train with a length of 200 pairs and pulse interval of 1 ms. (C) Sequence diagram for MT-3D-EPI. Image data from MT-prepared and control acquisition are acquired alternately and will be combined to generate the MT-weighted anatomical reference. In the MT-prepared image acquisition, binomial pulse train is applied before each excitation shot of 3D-EPI acquisition. In control condition, the sequence design is the same except that pulses in preparation are switched off.

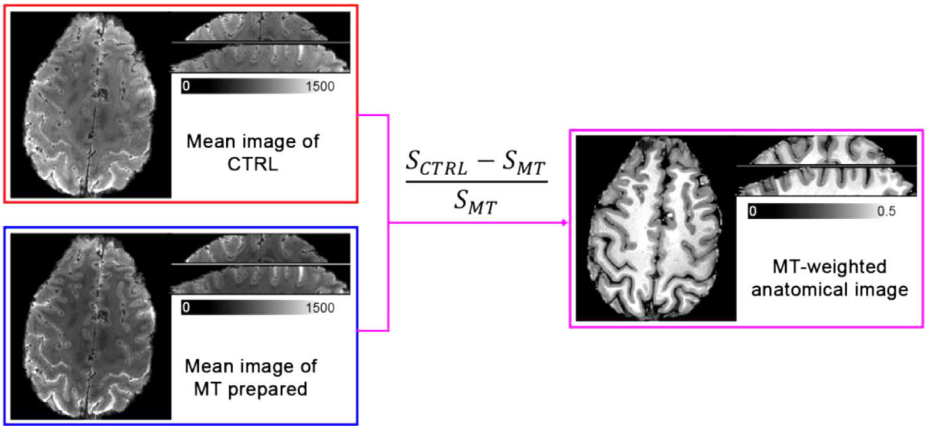

Fig. 2.

Generation of MT-weighted anatomical reference. We combined images of Control (CTRL, in red subpanel) and MT-prepared (in blue subpanel) through $\frac{S_{CTRL} - S_{MT}}{S_{MT}}$ to extract the MT saturated signal and remove the T_2* contrast associated with the EPI acquisition. The MT-weighted anatomical image has a clear contrast between GM and WM, while CSF and intravascular signals are both suppressed.

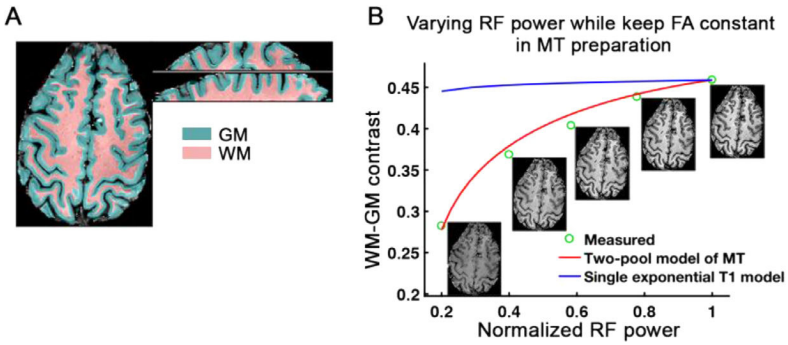

Fig. 3.

The WM-GM contrast under different RF powers of binomial pulse train. (A) Masks of GM and WM. (B) The WM-GM contrast as a function of normalized RF power of binomial pulses. WM-GM contrast was computed through $\frac{S_{WM} - S_{GM}}{(S_{WM} + S_{GM})/2}$. The green circle represents the measured WM-GM contrast, and their bellows show the corresponding MT-weighted EPI images. The red curve represents the WM-GM contrast predicted by the two-pool model of MT effect, while the blue curve represents the result predicted by the single exponential T1 relaxation model.

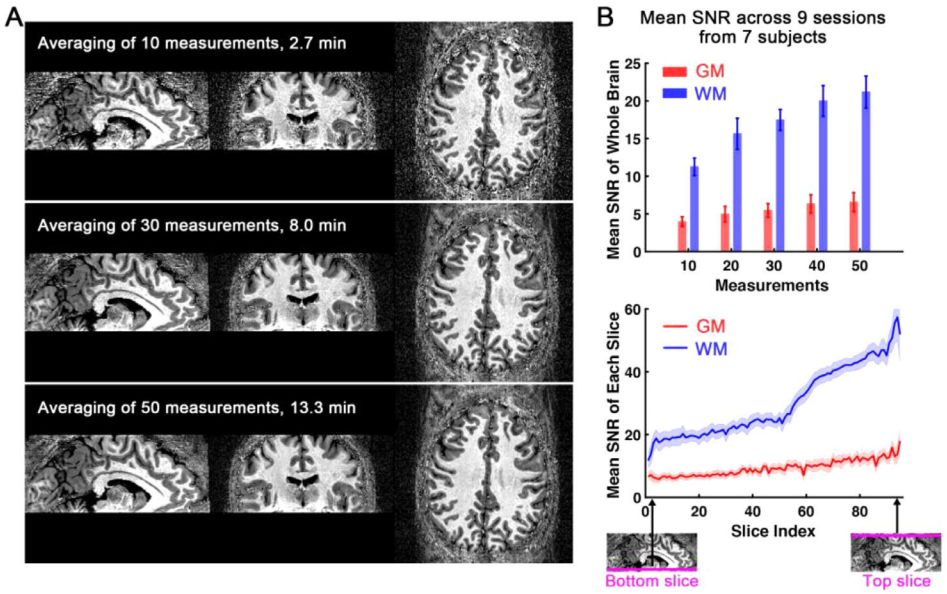

Fig. 4.

Anatomical MT-weighted EPI images and their SNRs after averaging different measurements. (A) Anatomical MT-weighted EPI images after averaging 10 (2.7 min), 30 (8 min) and 50 (13.3 min) measurements in one representative subject. (B) Group-mean SNR across 9 sessions from 7 subjects. Top: Mean SNRs of the whole-brain GM/WM regions in anatomical MT-weighted EPI images when averaging different measurements (10, 20, 30, 40, 50). Bottom: Mean SNRs of the GM/WM regions at different slices of the anatomical MT-weighted EPI images after averaging 50 measurements. With slice index increasing, slice position moves from the bottom to the top of the brain. All images and their SNR were computed before masking and denoising. Error bars represent ± the standard error of the mean (SEM) across sessions.

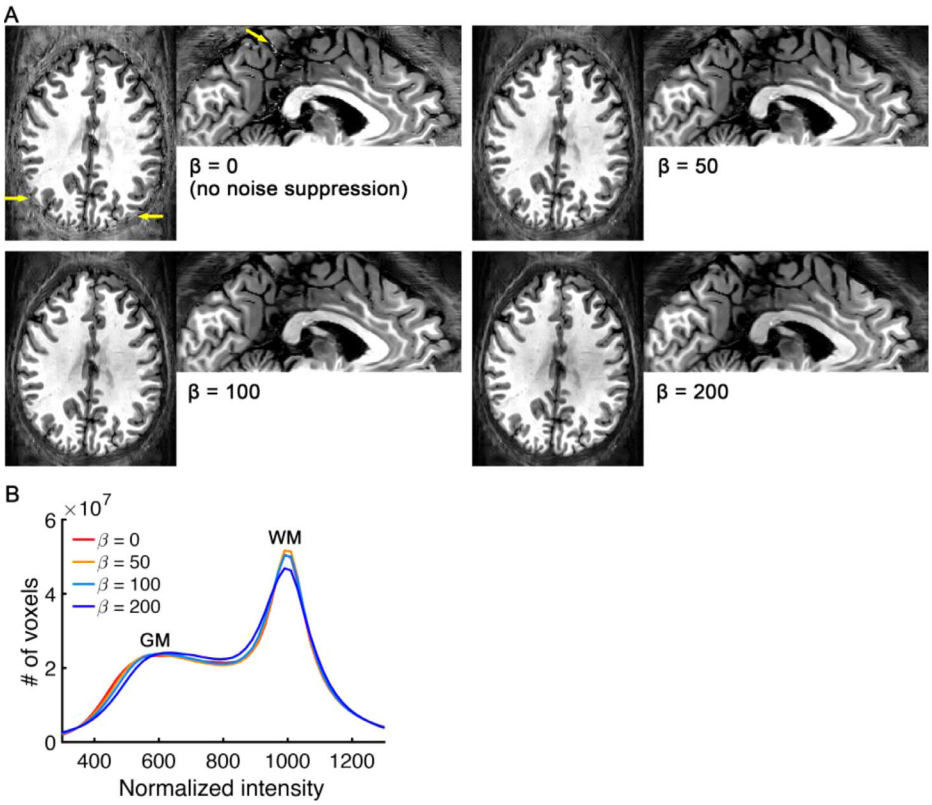

Fig. 5.

Background noise suppression. (A) Anatomical MT-weighted images were computed using equations of $S_{ANAT} = \frac{S_{CTRL} - S_{MT}}{S_{MT} + \beta}$ with $\beta = 0, 50, 100, 200$. In images of $\beta = 0$, noise signals were distributed across background non-brain region, in voxels non-cortical but touching cortical surface, and in some low-SNR brain voxels (a few examples marked by yellow arrows). With increasing β value, those noise signals can be better suppressed. (B) The histograms of the anatomical image intensities for voxels of the brain region across 9 sessions from 7 subjects at different β values. Larger β led to slightly worse separation of GM and WM intensity distribution (slightly worse GM/WM contrast).

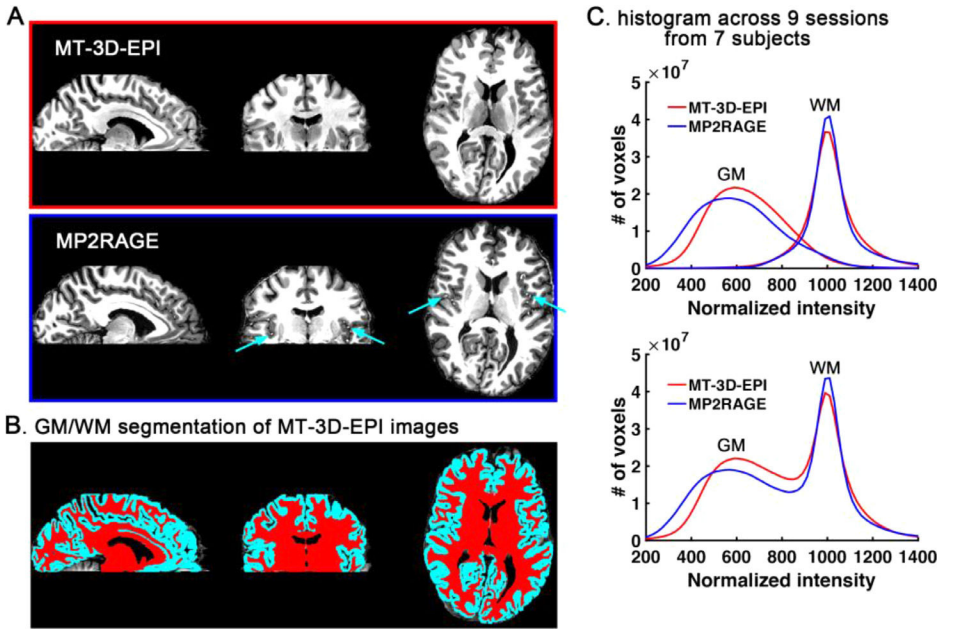

Fig. 6.

Near-whole-brain anatomical images and their histograms. (A) Top shows anatomical image acquired by MT-3D-EPI and bottom shows MP2RAGE image in one representative subject. (B) GM/WM segmentation of MT-weighted EPI image. (C) The histograms of image intensities for voxels within GM (lower values) and WM (higher values) (Top), and for voxels of the whole brain (Bottom) across 9 sessions from 7 subjects. The curves in red and blue represent the histograms acquired by MT-3D-EPI and MP2RAGE, respectively. The segmentation and histogram of CSF are separately shown in Fig. S1. (For interpretation of the references to color in this figure legend, the reader is referred to the web version of this article.)

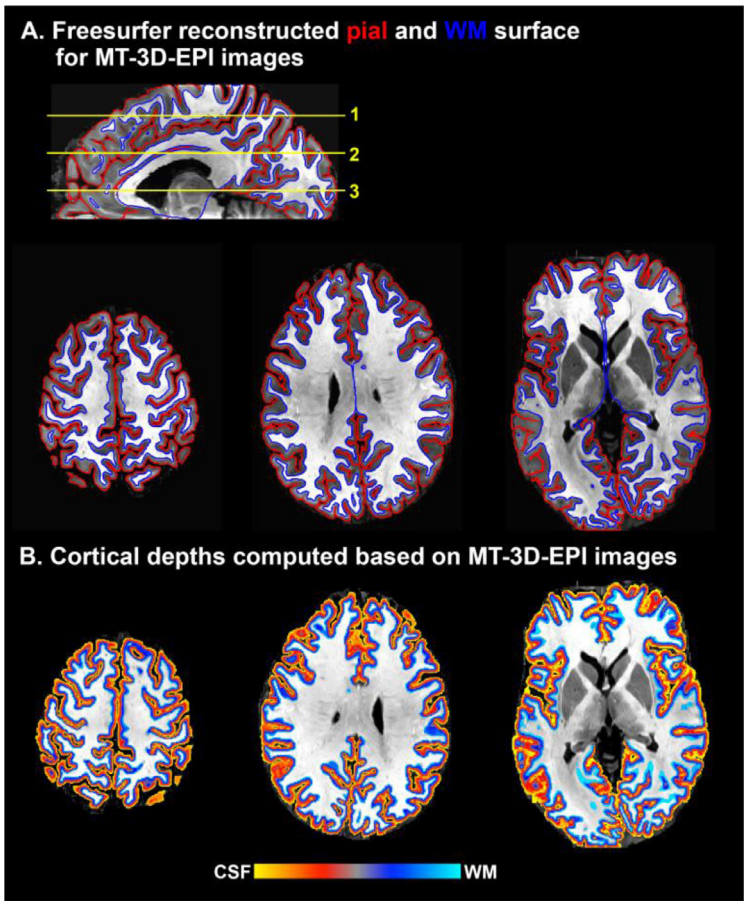

Fig. 7.

Cortical surface and layers generated based on the MT-weighted EPI image in one representative subject. (A) The underlay is the MT-3D-EPI acquired anatomical image and the overlay is the Freesurfer generated pial and WM surface based on it. The individual results of all remaining subjects are shown in Fig. S7. (B) Cortical depths were computed based on the cortical surfaces of the MT-weighted EPI image.

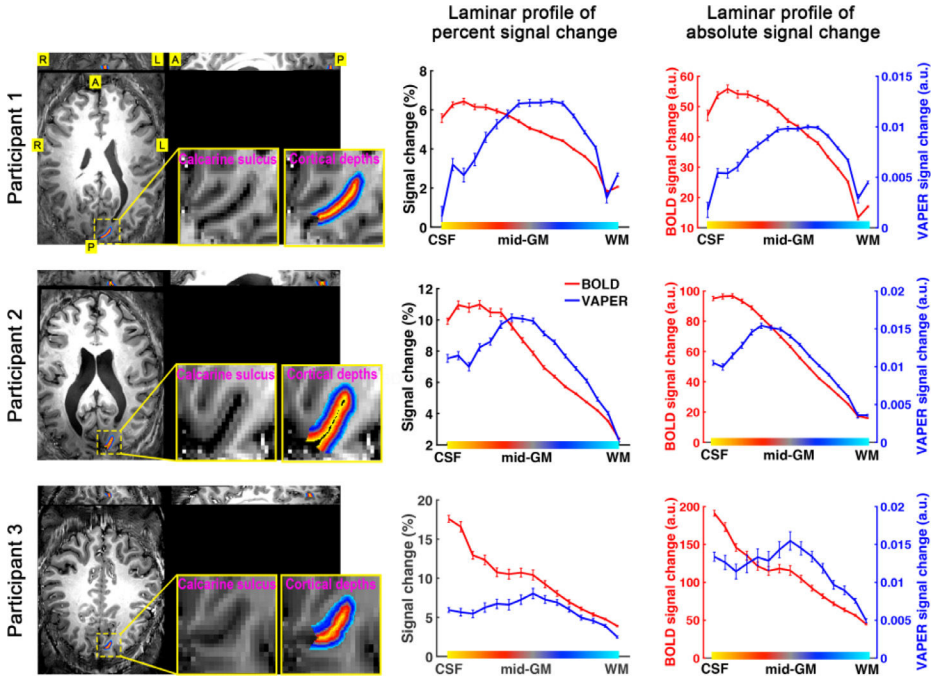

Fig. 8.

Cortical-depth dependent signal changes in native fMRI space. Rows refer to different participants. Left column: cortical depths (overlay) in calcarine sulcus were determined based on the MT-weighted EPI images (underlay). Middle column: laminar profiles of percent signal changes under BOLD (red curves) and VAPER (blue curves) contrasts to visual checkerboard stimulation. Right column: laminar profiles of absolute signal changes (arbitrary unit, a.u.) under BOLD (red curves) and VAPER (blue curves) contrasts to visual checkerboard stimulation. The percent signal changes were computed through normalizing to the mean signal of each voxel, while the absolute signal changes were computed without normalizing to the mean signal of each voxel.

Table 1

Scan parameters for MT-3D-EPI at 7T.

	Pulse #	Pulse FA	Pulse int. (ms)	Pulse dur. (us)	Res. (x × y × z mm^3)	Slice # (OS)	FOV read (mm)	FOV phase (%)	PF	TE (ms)	Volume TR (s)	Duty cycle of MT prep	Averages	Scan time (mm:ss)	Subjects/ Sessions
Exp. 1 (motor)	38	12°	1.1	120 to 900	0.8 × 0.8 × 0.9	28 (7.1%)	130	100	7/8	28	3.3	38%	83	09:08	3 sessions from 3 subjects
Exp. 2 (near-whole brain)	38	10.5°	0.2	150	0.8 × 0.8 × 0.84	96 (8.3%)	134	133	6/8	24	8	9.9%	52	13:52	9 sessions from 7 subjects
Exp. 3 (visual)	38	11.4	0.3	140	0.8 × 0.8 × 0.82	26 (7.7%)	133	133	6/8	24	3	10.6%	70	07:00	3 sessions from 3 subjects
Sup. Exp.	38	11.4	0.3	140	0.8 × 0.8 × 0.9	24 (8.3%)	130 or 142	100	7/8	28	3	9.9%	70	07:00	5 sessions from 3 subjects

Pulse # counts the MT preparation for only one segment. The pulse duration in Experiment 1 varied in a range of 120 to 900 ms to modulate the MT power (Power = FA^2 / Pulse_duration). Supplementary experiment (Sup. Exp.) was conducted to compare tissue contrast between MT-3D-EPI and T1-3D-EPI with a small brain coverage (24 slices), and details can be found in supplementary materials. FA – flip angle, int. – interval, dur. – duration, res. – resolution, # - number, PF – partial fourier, TE – echo time, volume TR – volume repetition time, OS – oversampling. Duty cycle of MT preparation was calculated as the percentage of the ratio of MT time to the total MT+EPI time.